Research article

Journal of RAMAN SPECTROSCOPY

Received: 28 February 2014 Revised: 15 May 2014 Accepted: 10 June 2014 Published online in Wiley Online Library: 11 July 2014

(wileyonlinelibrary.com) DOI 10.1002/jrs.4540

Effects of laser excitation wavelength and optical mode on Raman spectra of human fresh colon, pancreas, and prostate tissues

Ran Li,[a] Dominique Verreault,[a] Andrea Payne,[a] Charles L. Hitchcock,[b] Stephen P. Povoski,[c] Edward W. Martin Jr.[c] and Heather C. Allen[a,b]*

Early cancer detection is the central and most important factor for allowing successful treatment and resultant positive long-term patient outcomes. Recently, optical techniques have been applied to this purpose, although each has inherent limitations. In particular, Raman spectroscopy applied in the pathological diagnosis of cancerous tissues has received increasing attention, with the merit of being highly sensitive to the biochemical alterations in tissue compositions and applicable *in vivo*. Nevertheless, its application has been impeded by the high background intensity, which masks the Raman signal of biological molecules. In this work, the influence of laser excitation wavelength (785 *vs.* 830 nm) and optical mode (single mode *vs.* multimode) on the background intensity of fresh human tissues was studied. Based on the results, laser with 830 nm excitation demonstrated better background reduction than that with 785 nm excitation for the same optical mode, but the Raman signal intensity was conversely reduced, and the signal-to-noise ratio (SNR) not improved. In contrast, by comparing single-mode and multimode 785 nm excitations, it was shown that the single-mode laser with its smaller beam waist and beam propagation factor had better background reduction ability and an improvement of the SNRs. It is speculated that this decrease in background intensity comes from the effect of the optical mode on the Mie scattering from the biological tissue. High-quality spectra based on a careful selection of *both* laser excitation wavelength and optical mode will benefit Raman measurements in further research focusing on spectral interpretation and histopathological correlation ultimately aimed toward intraoperative applications. Copyright © 2014 John Wiley & Sons, Ltd.

Additional supporting information may be found in the online version of this article at the publisher's web site.

Keywords: cancer detection; single mode; multimode laser; 785 nm; 830 nm excitation

Introduction

Cancer is the second leading cause of mortality in the United States, just behind heart disease.[1] Based on the current data published by the American Cancer Society, there will be approximately 1 666 000 new cancer cases and 586 000 cancer deaths projected to occur in the United States in 2014.[2] Among all these cases, colorectal cancer is the third leading cause of cancer death in both men and women, whereas prostate cancer is the most frequently diagnosed cancer in men.[3] In view of the cancer prevalence in today's population, early cancer detection is crucial for allowing successful treatment and resultant positive long-term patient outcomes. Traditionally, the pathologic assessment of a resected tumor specimen relies on the judgment of the individual pathologists, which, however, can result in inconsistency in diagnosis. Furthermore, the final histopathological report is generally not available until many days after the performed surgical procedure. Taking this into consideration, there is a definite need for the development and/or application of highly sensitive, non-invasive techniques capable of identifying and distinguishing more quickly cancer-bearing tissues from non-cancer-bearing tissues. Such techniques could then potentially serve as extremely important adjunct methodologies to that of standard histopathological tissue analysis for real-time cancer detection as it relates to the assessment of surgical resection margins and the completeness of surgical resection in both the operating room and the pathology department.

In recent years, Raman spectroscopy has emerged as a technique that could potentially fulfill these requirements.[4–6] Numerous studies have shown that Raman spectroscopy can be a rapid and highly sensitive method for the detection of neoplastic tissue.[7–23] Furthermore, according to the Raman selection rule, water acts as a weak scatterer.[24–26] Because it does not suffer from any severe water interference from biological tissues, the technique is also readily applicable *in vivo*.[27] Finally, Raman spectroscopy requires little sample preparation because of the absence of any thickness restriction. Nevertheless, a widespread application of Raman spectroscopy in cancer detection and in the clinic in general has been hindered by some major drawbacks among which the high biological variability of different tissues and the great similarity of biological matter. Only recently could

* *Correspondence to: Heather C. Allen, Department of Chemistry and Biochemistry, The Ohio State University, 100 West 18th Avenue, Columbus, OH 43210, USA. E-mail: allen@chemistry.ohio-state.edu*

a *Department of Chemistry and Biochemistry, The Ohio State University, 100 West 18th Avenue, Columbus, OH, 43210, USA*

b *Department of Pathology, The Ohio State University, 129 Hamilton Hall, 1645 Neil Avenue, Columbus, OH, 43210, USA*

c *Division of Surgical Oncology, Department of Surgery, The Ohio State University, 410 West 10th Avenue, Columbus, OH, 43210, USA*

these limitations be dealt with using advanced statistical methods including principle component analysis, linear discrimination analysis, and cluster analysis.[28–30] Another even more serious problem comes from the presence of a strong background caused by tissue autofluorescence, which often masks the weak Raman scattering signal. To overcome this problem, different approaches have been explored on reducing tissue autofluorescence to improve the signal-to-noise ratio (SNR) including photolytic destruction of impurities,[31] use of excitation wavelengths in the near-infrared range,[12,16–18] and time-resolved detection.[32] However, among these methods, the latter two have mainly found wider application.

Using longer excitation wavelengths effectively reduces tissue autofluorescence background because there is less energy to excite electronic transitions in molecules.[16–18] However, it also decreases the Raman signal intensity as it is inversely proportional to the fourth power of the excitation wavelength. As a consequence, whether this method really helps with the improvement of the SNR needs to be further evaluated. In the case of time-resolved Raman spectroscopy, the longer-lived fluorescence ($\sim 10^{-8}$ s)[33] is typically filtered out from Raman scattering ($\sim 10^{-12}$ s)[34] by means of gated charge-coupled device (CCD) cameras. However, because accurate timing is difficult to be achieved on an ultrafast time scale, this approach usually requires sophisticated and expensive equipment.[22,32,35]

In this work, we investigate the combined effect of laser excitation wavelength and optical mode on the signal quality of Raman spectra from different fresh human tissues. Besides tissue autofluorescence, other potential sources of background in Raman spectra are examined. The effects of excitation wavelengths and optical modes on reducing background intensity are also discussed. The ultimate goal of this approach is to obtain the highest quality Raman spectra needed to generate a biochemical 'fingerprint'[36] of neoplastic tissue as compared with the adjacent normal tissue.

Experimental

Fresh tissue sampling

This study was approved by the Institutional Review Board (no. 2002H0089) of The Ohio State University Wexner Medical Center (OSUWMC). All human tissue specimens (i.e. colon, pancreas, and prostate; Fig. 1) utilized in this study were collected during a routine autopsy performed by the Department of Pathology at OSUWMC on an elderly man who had died from causes unrelated to cancer. The choice of the three different tissues was made to reflect some of the most prevalent cancer types in today's population. Without any need for additional tissue sectioning, the time spent on collecting and cutting tissues was quite short (~5 min). The thickness of collected colon, pancreas, and prostate specimens was typically 5–10 mm. Immediately after collection, tissue samples were brought to an adjacent laboratory for Raman spectroscopic measurements. In order to avoid defect-induced changes in the Raman spectra,[37] no fixation was used for any collected tissue specimen.

Raman measurements

The two-in-one setup used for Raman spectroscopy was built by coupling a Raman spectrometer (Dimension-P2, Lambda Solutions, Waltham, MA) with either an optical microscope or optical probes (Vector Raman Probe™, Lambda Solutions) as shown schematically in Fig. 1. Diode laser sources [785 nm single mode (785 SM) and multimode (785 MM), 830 nm multimode (830 MM); average power at the sample: ~35 mW] were used for excitation. A matching fiber optic probe (785 or 830 nm) was coupled to each laser source. Each probe contains a wavelength-matched laser line filter for excitation and a long-pass edge filter (785 nm RazorEdge® or 830 nm EdgeBasic™, Semrock, Rochester, NY; $\lambda_{edge} = 791.6$ or 846 nm, $OD_{abs} > 6$ for $\lambda > 785$ or 830 nm, diam. 25.4 mm). The beam propagation factor (M^2) for the 785 SM, 785 MM, and 830 MM is 1.1, 1.6−2, and 2, respectively. The bandwidths for the single-mode and multimode lasers are 0.001 and 0.1 nm, respectively. The beam waist (W_0) for the multimode beam is 25–30 μm, while the single-mode beam is about 30 times smaller. Each probe was connected to a 33-fiber array (50 μm) coupled to the Dimension-P2 spectrometer by a bundle-to-slit (50 μm) configuration. The Raman scattering light in the spectrometer was collected by a collimating lens (Nikon, Melville, NY; *f*/1.8 85 mm), passed through a second long-pass edge filter (785 nm RazorEdge®, Semrock; diam. 50.8 mm). The collimated light was reflected on a gold-enhanced mirror (Edmund Optics) and dispersed by a holographic reflection grating (1800 grooves/mm, Optometrix, Ayer, MA). The dispersed light was focused onto a back-illuminated, thermoelectrically cooled CCD camera (Critical Link, Syracuse, NY; 128 × 1024 pixels, 24 μm × 24 μm pixel size) with an *f*/1.8, 85 mm lens (Nikon). Spectra were collected using the RamanSoft™ acquisition software (v. 1.4.2, Lambda Solutions). All Raman measurements were performed using a backscattering geometry. For each investigated tissue specimen, two representative spots were selected out of a sampling of locations ($n = 5$–10): one yielding the best SNR among all locations (referred hereafter to as 'hot spot') and another chosen randomly (referred to as 'random spot'). The exposure time of the CCD was set to 2 s with 40 accumulations, which gave an overall acquisition time of 80 s per spectra. A larger number of accumulations were chosen to improve the SNR. Note that the data reported in this paper were obtained for all tissues over a 1-day time period to minimize experimental parameters. However, over a period of 1 year, many replicate spectra from multiple tissues and tissue types have been performed. Statistical analysis has shown that SNR standard deviation remains small such that the selection of one spectral data set per location is sufficient and adequate.

Data processing

In order to correct for residual CCD etaloning and wavelength sensitivity, a broadband spectrum was obtained with a calibration standard (LS-1-CAL tungsten halogen light source, Ocean Optics, Dunedin, FL). The spectrum was then fitted by an eighth-order polynomial function. The broadband spectrum was normalized by dividing by the polynomial curve to obtain a set of correction factors at each pixel. These factors were then applied at each point of the raw Raman spectrum for etaloning correction by an automatic etalon correction factor built into RamanSoft™. The etaloning correction procedure was similar to the one developed by Vickers *et al.* for noise removal[38] and was performed with custom-built routines written in Origin (v. 8.0, OriginLab, Northampton, MA) and MATLAB (v. 11.0, MathWorks, Natick, MA) softwares. To correct for the intensity (CCD wavelength sensitivity), the polynomial curve was

Journal of RAMAN SPECTROSCOPY

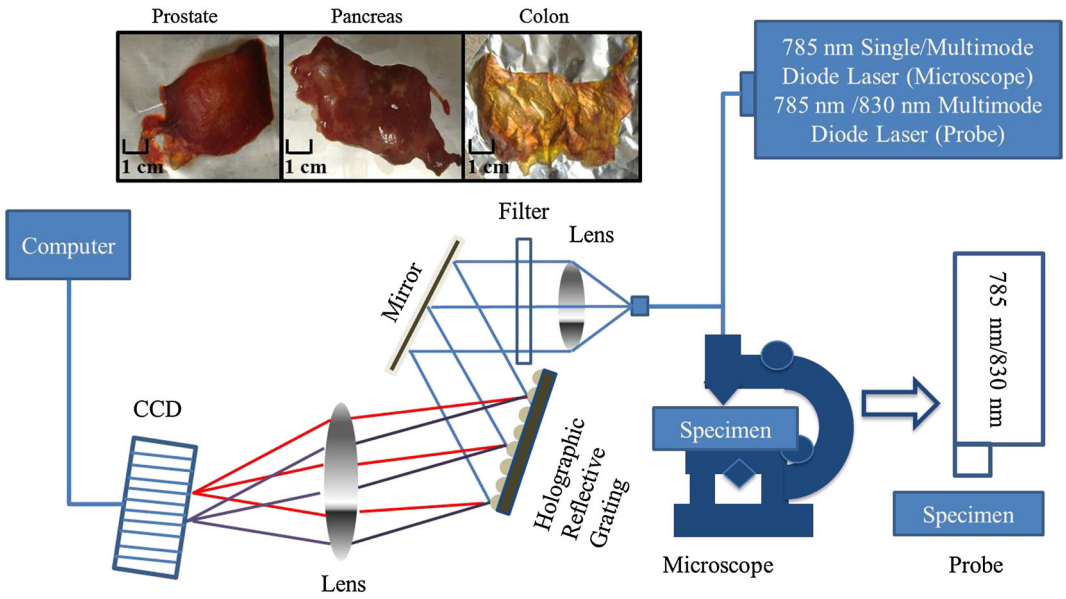

Figure 1. Block diagram of Dimension-P2 Raman spectrometer coupled with either microscope or probes. Photographs of human tissue specimens are also shown (upper right).

normalized to unity by dividing through its maximum value, and then, the etaloning-corrected spectrum was divided by the new curve for intensity normalization. Note that the fiber optic and the probe head were utilized for normalization as well such that direct comparison between the different wavelength excitation and the modes was feasible. The intensity correction procedure was performed with custom-built routines written in MATLAB.

Additionally, because the Raman spectrometer is designed for the 785 nm excitation, the Raman shift had to be recalculated when applying the 830 nm excitation. Therefore, Raman spectra obtained with the latter wavelength have a spectral cutoff above 2348 cm^{-1}. The background signal present in the etaloning-corrected and intensity-corrected Raman spectra was removed by applying a set of baseline corrections over different spectral regions of the 1024 data points. Seven to 11 points were applied to draw the baselines depending on the spectra using the manual baseline correction tool in RamanSoft™. Finally, the SNR calculations were performed via custom-built routines developed in MATLAB. An example of SNR calculations for the amide I band (~1650 cm^{-1}) can be found in the supporting information.

Experimental results

Effect of wavelength

Figure 2 shows the comparison between the raw Raman spectra obtained with two different excitation wavelengths but with the same optical mode (785 MM and 830 MM) on hot and random spots of colon, pancreas, and prostate tissue specimens. For each tissue, the background-corrected Raman spectra over the fingerprint and amide I spectral regions (1200–1800 cm^{-1}) are also given (shown as insets in Fig. 2). As seen in the raw Raman spectra of the colon tissue specimen [Fig. 2(a and b)], backgrounds with 785 MM are approximately the same on the random and hot spots, and 830 MM yields lower background signal than 785 MM on both spots. After background correction, the Raman signals are found to be higher with 785 MM than with 830 MM on both hot and random spots, although Raman intensities on the random spot are two to three times lower than those on the hot spot. For the raw Raman spectra obtained from the pancreas tissue specimen [Fig. 2(c and d)], 830 MM also generated lower backgrounds than 785 MM on both hot and random spots; however, the signal intensity was lower on the random spot than on the hot spot for 785 MM and, vice versa, for 830 MM. As for the background-corrected spectra, the Raman signals are higher on the hot spot than on the random spot, and 785 MM yields higher Raman signals than 830 MM on both hot and random spots. Finally, in the case of the prostate tissue specimen, the raw Raman spectra [Fig. 2(e and f)] show slightly higher backgrounds (~1.2–1.5 times) on the random spot than on the hot spot. In addition, 830 MM yields lower background signals than 785 MM on both hot and random spots. Similar to the two other tissues, the background-corrected Raman spectra exhibit higher signals on the hot spot than on the random spot, especially with 785 MM.

Overall, the raw Raman spectra taken with 830 MM have lower backgrounds than those with 785 MM. However, the Raman signals in the background-corrected spectra are also reduced by using 830 MM as wavelength. The background intensities vary from tissue to tissue on the hot and random spots, but the Raman signal intensities are always higher on the hot spot regardless of the wavelength, as expected. In order to better analyze the data, a quantitative analysis was conducted by calculating the SNR of the well-known amide I band at ~1650 cm^{-1} [Table S1 (supporting information)]. Between different wavelengths (but same optical mode), one sees that for the colon tissue specimen, the SNR with 785 MM is about 1.6 times higher than that with 830 MM on both hot and random spots (Table 1). For each wavelength, however, the SNR on the hot spot is about 2.1 times higher than that on the random spot. Similarly, for the pancreas tissue specimen, the SNR with 785 MM is about 1.3 times higher than that with 830 MM on both spots, whereas the SNR values for both wavelengths are about 1.4 times higher on the hot spot than on the random spot. Finally, with the prostate tissue, the SNR with 785 MM is about 1.2 and 1.6 times higher than that with 830 MM on the hot and random spots, respectively. The SNRs

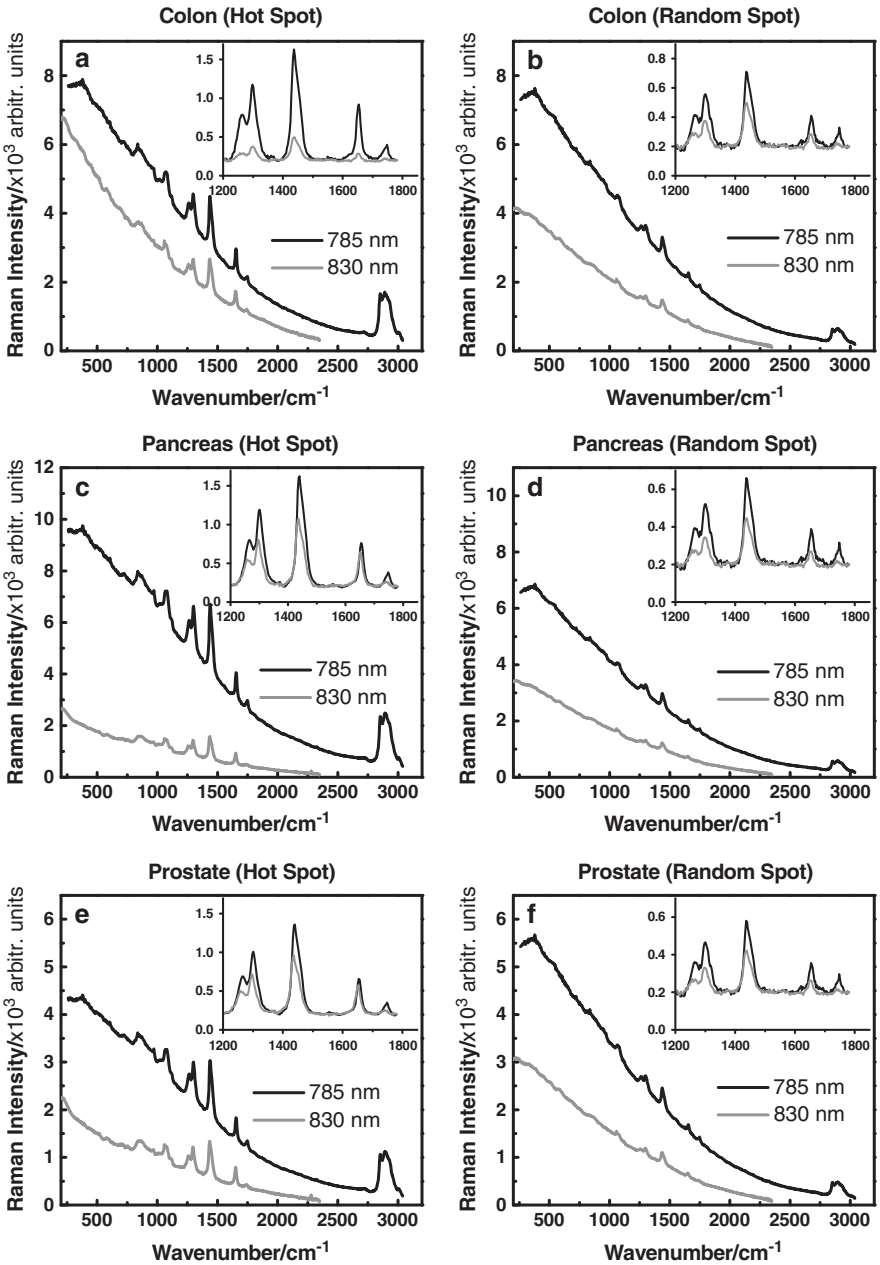

Figure 2. Raman spectra of tissue specimens with 785 MM and 830 MM. Colon, pancreas, and prostate (a, c, e) hot and (b, d, f) random spots.

obtained with 785 MM and 830 MM on the hot spot are almost identical with those on the random spot, respectively. Taken together, these results indicate that (1) the hot spot yields higher SNRs than the random spot, independent of the chosen wavelength, and (2) the Raman spectra with 785 MM have higher SNRs than those with 830 MM, regardless of the tissue type and probing location.

Effect of optical mode

To assess the effect of optical mode on the Raman response of biological tissues, Fig. 3 presents the raw Raman spectra obtained with two different optical modes but with the same excitation wavelength, 785 SM and 785 MM, on the same tissue specimens previously used. The Raman band assignment of colon tissue taken with 785 SM [Fig. S2 (supporting information)] is given in Table S1. Again, for each tissue specimen, the raw and background-corrected Raman spectra (see insets of Fig. 3) are given on both hot and random spots. For the colon tissue specimen, the raw Raman spectra [Fig. 3(a and b)] show that the background intensities are much higher (up to approximately five times) on the random spot than on the hot spot for both 785 SM and 785 MM. However, 785 SM yields slightly lower backgrounds (~1.1–1.3 times less) than 785 MM on both hot and random spots. As for the background-corrected Raman spectra, the Raman signals with 785 SM and 785 MM are practically indistinguishable on both hot and random spots. In the case of the pancreas tissue specimen, the raw Raman spectra exhibit backgrounds with both 785 SM and 785 MM that are also higher on the random spot than on the hot spot, although to a lesser extent than with the colon tissue [Fig. 3(c and d)]. Moreover, 785 SM yields lower backgrounds than 785 MM on both hot and random

Journal of RAMAN SPECTROSCOPY

Table 1. Raman signal-to-noise ratio of the amide I band (~1650 cm^{-1}) on the hot and random spots for different tissue specimens

Tissue	785 SM	785 MM		785 MM	830 MM	
Colon						
Hot	97.9	87.0	**1.1**	76.6	48.0	**1.6**
Random	46.7	41.4	**1.1**	60.0	36.6	**1.6**
	1.3	**1.3**		**2.1**	**2.1**	
Pancreas						
Hot	107.9	57.9	**1.9**	73.0	57.2	**1.3**
Random	93.6	36.2	**2.6**	53.9	42.1	**1.3**
	1.4	**1.4**		**1.2**	**1.6**	
Prostate						
Hot	79.1	66.7	**1.2**	77.8	67.2	**1.2**
Random	70.3	63.7	**1.1**	71.2	45.2	**1.6**
	1.1	**1.5**		**1.1**	**1.0**	

SM, single mode; MM, multimode.

spots. In the background-corrected Raman spectra, the Raman signals are clearly higher on the hot spot than on the random spot, but the Raman signals with 785 SM and 785 MM have practically equal intensities on both hot and random spots. Finally, with the prostate tissue specimen, the raw Raman spectra show approximately equal background levels for 785 MM on the random and hot spots [Fig. 3(e and f)]. In contrast, for 785 SM, the background signal is lower on the random spot (by about a factor 1.5) compared with the hot spot. Also, 785 SM yields lower backgrounds than 785 MM but only on the random spot; on the hot spot, backgrounds are nearly identical for 785 SM and 785 MM, except at lower wavenumbers (<1000 cm^{-1}). As for the background-corrected Raman spectra, the Raman signals are slightly higher on the random spot compared with the hot spot. In addition, the Raman signals with 785 SM and 785 MM are of equal intensities on the hot spot.

Overall, the raw Raman spectra with 785 SM have lower backgrounds than those with 785 MM, although the decrease is less pronounced than the one observed between different wavelengths (Fig. 2). The background-corrected Raman signals are nearly equal in intensity for both modes. Like in Fig. 2, the background levels vary from tissue to tissue on the hot and random spots. From the quantitative analysis, the SNR from the colon tissue with 785 SM is about 1.1 times higher than that with 785 MM on both hot and random spots (Table 1). For the same optical mode, the SNR on the hot spot is about 1.3 times higher than that on the random spot. In the case of the pancreas tissue specimen, the optical mode effect is more pronounced with SNR values using 785 SM, about 1.9 and 2.6 times higher than with 785 MM on the hot spot and random spot, respectively. The SNR values with 785 SM and 785 MM on the hot spot are comparable, being about 1.4 times higher, than on the random spot. Finally, with the prostate tissue, the SNR with 785 SM is about 1.2 and 1.1 times higher than that with 785 MM on the hot and random spots, respectively. Like the two other tissues, for the same optical mode, the SNR values remain almost unchanged between hot and random spots (~1.3 times higher on average). Based on this analysis, the hot spot yields comparable or higher SNRs than the random spot. Furthermore, regardless of tissue type, it seems that choosing 785 SM over 785 MM not only reduces the background but also improves the SNR.

Discussion

As mentioned earlier, the widespread clinical use of Raman spectroscopy, particularly in cancer detection, has been impeded by some major drawbacks among which the presence of tissue autofluorescence. Because most biological molecules have a large number of carbonyl groups and aromatic ring structures, these can act as endogenous fluorophores when excited in the visible wavelength range (typically, in the range of 200–500 nm[39]). Fluorescence then occurs as a result of electrons relaxing back from an excited state to the ground state and competes against Raman scattering. Additionally, the cross sections for fluorescence and Rayleigh scattering are 10^{-16} and 10^{-26} cm^2,[40] respectively, whereas that for Raman scattering is smaller yet with 10^{-29} cm^2,[41] thus making tissue autofluorescence more likely to occur than Raman scattering. Besides autofluorescence, the potential risk of induced tissue photodamage also somewhat prohibits the extensive use (e.g. too long exposure times) of shorter wavelengths on biological tissues.

The choice of longer excitation wavelengths (>700 nm) thus constitutes an obvious option when it comes to reducing the background signal due to tissue autofluorescence because they are less energetic and thus less susceptible to excite electronic transitions in fluorophores. For instance, 830 and 1064 nm excitation wavelengths have commonly been used as substitutes for 785 nm.[12,16–18] Similarly, it was shown in the previous section that the backgrounds observed with 830 MM are lower than those obtained with 785 MM, regardless of the tissue type and probing location on the tissue. Unfortunately, because the Raman signal intensity is inversely proportional to the laser excitation wavelength,[42] 830 MM also reduces the Raman signals compared with 785 MM. Hence, although 830 MM demonstrates better autofluorescence reduction than 785 MM, the SNRs are not improved in spectra taken with 830 MM (Table 1). Therefore, applying longer excitation wavelength for improving SNR is not so advantageous on account of substantial reduction in Raman signal intensity.

If autofluorescence is the only source responsible for the background, then single-mode and multimode lasers should have similar background intensity; however, results presented above showed that this is not the case. There must be some other contributions to the background besides autofluorescence. One of these sources could be the scattering generated by the inhomogeneity in the tissue structures. Depending on the size of these structures relative to the excitation wavelength, one of two types of scattering can occur, namely Rayleigh (and Raman) and Mie scatterings. The sizes of some structures including membranes, cellular subcompartments, and ultrastructure of collagen fibrils are beyond the range of the currently used excitation wavelengths. Here, Rayleigh scattering and its related process, Raman scattering, take place. However, sizes of most components are close to or larger than both 785 and 830 nm laser excitation wavelengths. As a consequence, Mie scattering occurs instead of Rayleigh scattering. The intensity of the Mie scattering is defined as[43]

$$I(\theta) = I_0 \frac{\pi a^2 Q_s p(\theta)}{4\pi r^2} \quad (1)$$

where a is the size of the scatterer, Q_s is the scattering efficiency, $p(\theta)$ is the normalized phase function, and r is the distance between the scatterer and the observer. As seen in Eqn 1, Mie

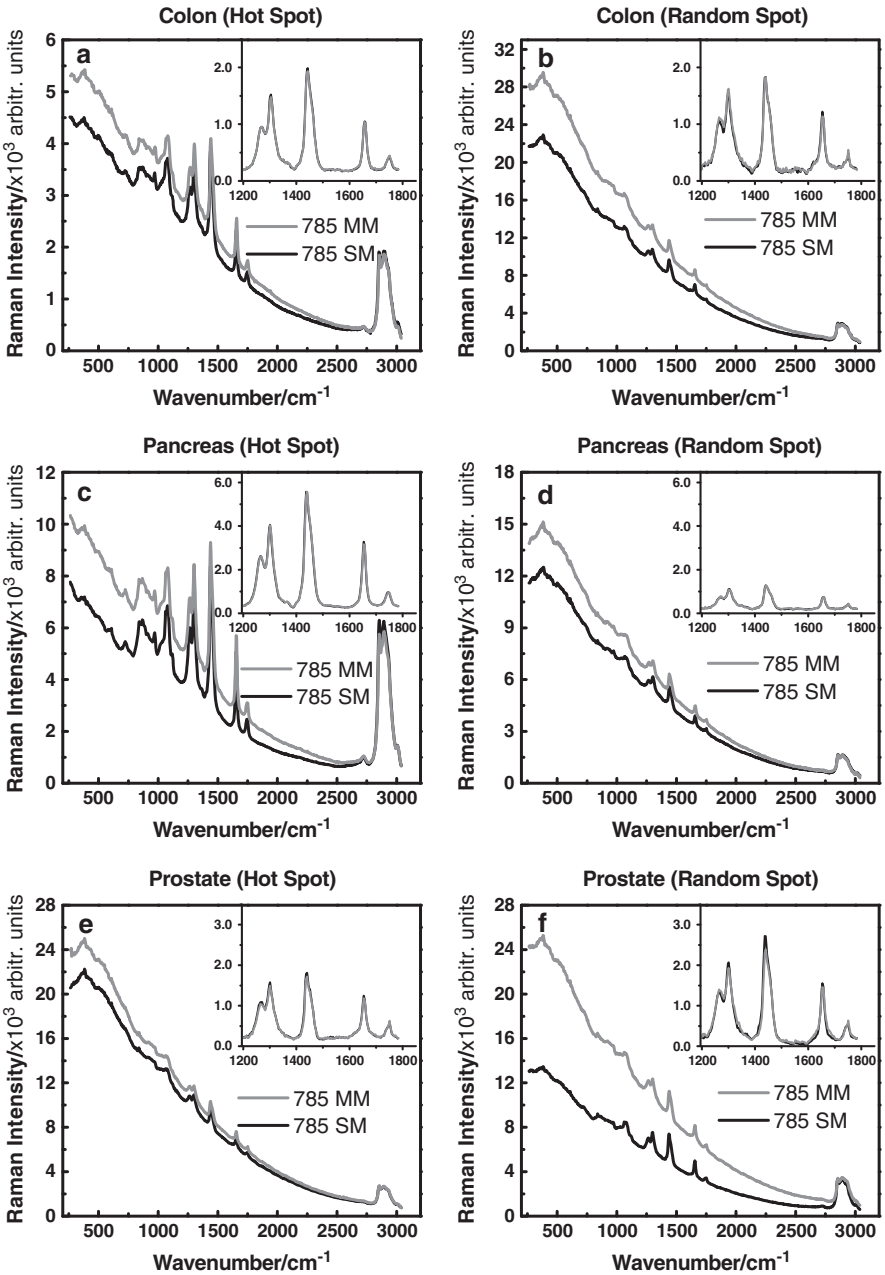

Figure 3. Raman spectra of tissue specimens with 785 SM and 785 MM. Colon, pancreas, and prostate (a, c, e) hot and (b, d, f) random spots.

scattering is size dependent but insensitive to the excitation wavelength. Consequently, 830 MM does not help in reducing the background arising from Mie scattering.

For example, mitochondrion, an important cellular organelle whose function is to furnish energy to the cell, has a characteristic size that varies between 0.5 and 2 μm in diameter, depending on the cell type. This organelle is enclosed by a lipid bilayer and has additional lipid bilayers that separate different internal compartments. Because of this dramatic optical contrast with their surroundings, mitochondria act as a dominant Mie scattering source. Other organelles giving rise to Mie scattering include lysosomes, peroxisomes (0.25–0.5 μm in diameter) secreted by the endoplasmic reticulum and Golgi apparatus, and the largest cellular organelle, the cell nucleus (4–6 μm in diameter).[44] The cross section for Mie scattering in biological tissue is quite large (~10^{-16} cm^2) and within the range of that of fluorescence (10^{-26}–10^{-8} cm^2).[41,42] In addition, because of the heterogeneous nature of biological tissues, which can be regarded as 'turbid media',[45] light propagation here cannot simply be described by assuming isolated, non-interacting scatterers, where scattering fields do not interfere with each other. Therefore, one should

Table 2. Beam propagation factor (M^2), beam waist (W_0), and divergence angle (ϑ) of 785 SM, 785 MM, and 830 MM

Beam parameter	785 SM	785 MM	830 MM
M^2	1.1	1.6–2.0	2.0
W_0 (μm)	0.8–1.0	25–30	25–30
ϑ (°)	63.0–73.2	3.1–4.6	4.0–4.9

SM, single mode; MM, multimode.

Journal of RAMAN SPECTROSCOPY

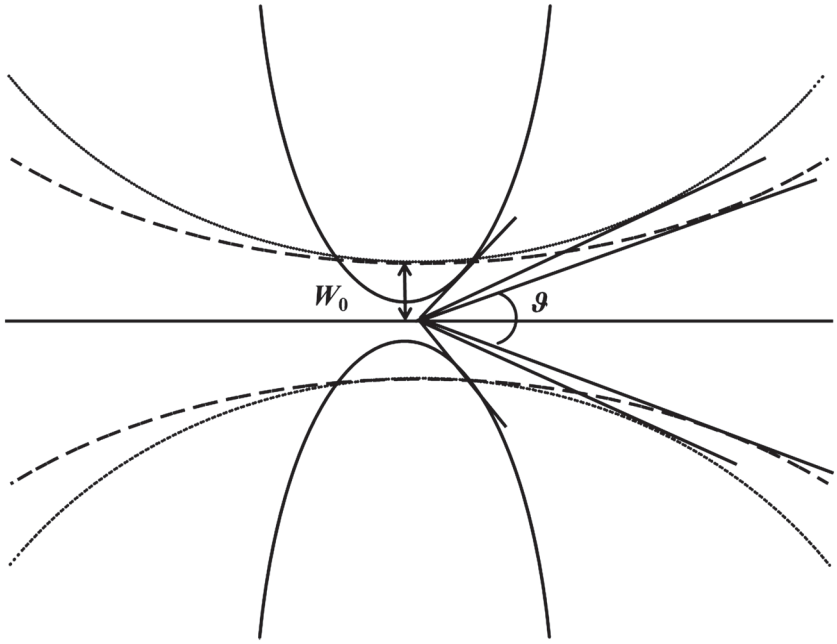

Figure 4. Sketch of the beam profiles of 785 SM (solid line), 785 MM (dashed line), and 830 MM (dotted line). W_0 and ϑ refer here to the beam waist and divergence angle, respectively.

rather view the Mie scattering in biological tissue more as a 'multiple Mie scattering'. Hence, a plausible mechanism that could explain the contribution of Mie scattering to the background intensity could be that the Mie response, which is backscattered in many angular directions, cannot be completely filtered out. The reason for this is that the interference filters used to block the elastic scattering are not as efficient when light enters at any angle other than normal to the filter surface, such that part of this scattering could make its way into the monochromator. Once inside the monochromator, multiple input angles also give rise to signal that shows up as different wavelength contributions.

Another possible explanation for the difference in background intensity could come from the beam profile of the different light sources. For a real, non-diffraction-limited beam, the divergence angle is given by

$$\vartheta = M^2 \frac{4\lambda}{\pi W_0} \tag{2}$$

where W_0 is the beam waist and M^2 is the beam propagation factor, which is used to determine how much the laser beam angle departs from its theoretical value.[46–48] The beam propagation factor, beam waist, and divergence angle of 785 SM, 785 MM, and 830 MM are summarized in Table 2. Based on these parameters, the beam profiles of 785 SM, 785 MM, and 830 MM are sketched schematically in Fig. 4.

When comparing the different modes with the same 785 nm excitation wavelength, 785 MM has a larger beam waist but less beam divergence than 785 SM. Despite this large difference in beam waist, Raman signals with 785 SM and 785 MM are nearly equal. This is because the laser power and, in turn, the number of photons incident on the tissue surface with 785 SM and 785 MM are equal. Because the beam waist of 785 MM is larger than that of 785 SM, more area is illuminated by the former, resulting in more background due to Mie scattering.

From the comparison between different excitation wavelengths with the same optical mode, 830 MM has a larger divergence angle than 785 MM (Table 2). As a consequence, 830 MM yields more Mie scattering than 785 MM. However, because the difference in the divergence angle between 785 MM and 830 MM is negligible, the increase in Mie scattering background with 830 MM should be insignificant. Furthermore, as discussed earlier, 830 MM reduced the tissue autofluorescence; therefore, an increase in Mie scattering should not be a major issue when applying 830 MM excitation.

Conclusions

The results obtained in this study demonstrate that the high background intensity in the Raman spectra of fresh tissue can be reduced following two possible approaches. The first and already known approach consists in applying longer excitation wavelengths, preferably closer to the near-infrared range. The effect of the excitation wavelength on the background signal was clearly demonstrated by comparing between 785 MM and 830 MM. However, a well-known drawback of this approach is that the Raman signal and the SNR are concomitantly reduced. Another, perhaps, less studied approach, based on the selection of the laser optical mode (single mode *vs.* multimode), has been shown to reduce part of the background possibly due to Mie scattering. A comparison of 785 SM and 785 MM has revealed that single-mode source not only reduces the background intensity but also improves the SNR. Taken together, these results suggest that an improvement of fresh tissue Raman spectra quality could come from the careful selection of both laser excitation wavelength and optical mode. The outcome of this study will certainly help in the application of Raman mapping of fresh biological tissues and in the use of statistical analysis algorithms enabling the identification of potential tissue-specific and/or oncogenic biomarkers.[49]

Acknowledgements

The authors gratefully acknowledge the National Cancer Institute and the National Institutes of Health (NIH R21 CA 167403), Victor Sapirstein (Lambda Solutions, Inc.) for his help with the RamanSoft™ software package and instrumentation, and The Ohio State University Wexner Medical Center's Autopsy Services for facility support.

References

[1] M. Heron, *Natl. Vital Stat. Rep.* **2013**, *62*, 1.
[2] R. Siegel, J. Ma, Z. Zou, A. Jemal, *CA Cancer J. Clin.* **2014**, *64*, 9.
[3] American Cancer Society, Cancer Facts & Figures 2014, American Cancer Society, Atlanta, **2014**.
[4] R. Thomas, K. Bakeev, M. Claybourn, R. Chimenti, *Spectroscopy* **2013**, *28*, 36.
[5] Z. Movasaghi, S. Rehman, I. U. Rehman, *Appl. Spectrosc. Rev.* **2007**, *42*, 493.
[6] P. Matousek, *Chem. Soc. Rev.* **2007**, *36*, 1292.
[7] J. Zhao, H. Lui, D. I. McLean, H. Zeng, in Real-Time Raman Spectroscopy for Noninvasive in vivo Skin Analysis and Diagnosis, (Ed. D. Campolo), IN-TECH, Vienna, **2010**, pp. 455–474.
[8] S. Duraipandian, M. S. Bergholt, W. Zheng, K. Y. Ho, M. Teh, K. G. Yeoh, J. B. Y. So, A. Shabbir, Z. W. Huang, *J. Biomed. Opt.* **2012**, *17*, 8.
[9] Y. Z. Li, J. J. Pan, G. N. Chen, C. Li, S. J. Lin, Y. H. Shao, S. Y. Feng, Z. F. Huang, S. S. Xie, H. S. Zeng, R. Chen, *J. Biomed. Opt.* **2013**, *18*, 027003-1.
[10] C. A. Patil, I. J. Pence, C. A. Lieber, A. Mahadevan-Jansen, *Opt. Lett.* **2014**, *39*, 303.
[11] M. V. P. Chowdary, K. K. Kumar, K. Thakur, A. Anand, J. Kurien, C. M. Krishna, S. Mathew, *Photomed. Laser Surg.* **2007**, *25*, 269.
[12] P. Crow, B. Barrass, C. Kendall, M. Hart-Prieto, M. Wright, R. Persad, N. Stone, *Br. J. Cancer* **2005**, *92*, 2166.
[13] P. Crow, A. Molckovsky, N. Stone, J. Uff, B. Wilson, L. M. Wongkeesong, *Urology* **2005**, *65*, 1126.
[14] P. Crow, N. Stone, C. A. Kendall, J. S. Uff, J. A. M. Farmer, H. Barr, M. P. J. Wright, *Br. J. Cancer* **2003**, *89*, 106.
[15] Z. W. Huang, A. McWilliams, H. Lui, D. I. McLean, S. Lam, H. S. Zeng, *Int. J. Cancer* **2003**, *107*, 1047.
[16] S. Kaminaka, H. Yamazaki, T. Ito, E. Kohda, H. O. Hamaguchi, *J. Raman Spectrosc.* **2001**, *32*, 139.
[17] T. Kawabata, T. Mizuno, S. Okazaki, M. Hiramatsu, T. Setoguchil, H. Kikuchi, M. Yamamoto, Y. Hiramatsu, K. Kondo, M. Baba, M. Ohta, K. Kamiya, T. Tanaka, S. Suzuki, H. Konno, *J. Gastroenterol.* **2008**, *43*, 283.
[18] Y. K. Min, T. Yamamoto, E. Kohda, T. Ito, H. Hamaguchi, *J. Raman Spectrosc.* **2005**, *36*, 73.
[19] A. Molckovsky, L. Song, M. G. Shim, N. E. Marcon, B. C. Wilson, *Gastrointest. Endosc.* **2003**, *57*, 396.
[20] S. K. Teh, W. Zheng, K. Y. Ho, M. Teh, K. G. Yeoh, Z. Huang, *Br. J. Cancer* **2008**, *98*, 457.
[21] S. K. Teh, W. Zheng, K. Y. Ho, M. Teh, K. G. Yeoh, Z. W. Huang, *J. Biomed. Opt.* **2008**, *13*, 034013-1.
[22] D. L. Andrews, A. A. Demidov, An Introduction to Laser Spectroscopy, Kluwer Academic/Plenum Publishers, New York, **2002**.
[23] C. A. Lieber, S. K. Majumder, D. L. Ellis, D. D. Billheimer, A. Mahadevan-Jansen, *Lasers Surg. Med.* **2008**, *40*, 461.
[24] H. Barańska, A. Łabudzińska, J. Terpiński, Laser Raman Spectrometry: Analytical Applications, Polish Scientific Publishers, Warsaw, **1987**.
[25] M. J. Pelletier, Analytical Applications of Raman Spectroscopy, John Wiley & Sons, New York, **1999**.
[26] M. Ren, Comparison of Near Infrared and Raman Spectroscopies for Noninvasive Clinical Measurements, PhD Thesis, University of Iowa, Iowa City, **2007**.
[27] C. Kendall, M. Isabelle, F. Bazant-Hegemark, J. Hutchings, L. Orr, J. Babrah, R. Baker, N. Stone, *Analyst* **2009**, *134*, 1029.
[28] C. M. Krishna, G. D. Sockalingum, R. A. Bhat, L. Venteo, P. Kushtagi, M. Pluot, M. Manfait, *Anal. Bioanal. Chem.* **2007**, *387*, 1649.
[29] F. Severcan, P. I. Haris, Vibrational Spectroscopy in Diagnosis and Screening, IOS Press, Amsterdam, **2012**.
[30] Y. Oshima, H. Shinzawa, T. Takenaka, C. Furihata, H. Sato, *J. Biomed. Opt.* **2010**, *15*, 017009-1.
[31] D. P. Strommen, K. Nakamoto, Laboratory Raman Spectroscopy, John Wiley & Sons, New York, **1984**.
[32] D. V. Martyshkin, R. C. Ahuja, A. Kudriavtsev, S. B. Mirov, *Rev. Sci. Instrum.* **2004**, *75*, 630.
[33] J. R. Lakowicz, Principles of Fluorescence Spectroscopy, Springer Verlag, New York, **2006**.
[34] I. R. Lewis, H. G. M. Edwards, Handbook of Raman Spectroscopy: From the Research Laboratory to the Process Line, Taylor & Francis, New York, **2001**.
[35] P. D. Peter Lasch, P. D. Janina Kneipp, Biomedical Vibrational Spectroscopy, John Wiley & Sons, New York, **2008**.
[36] F. M. Lyng, E. O. Faolain, J. Conroy, A. D. Meade, P. Knief, B. Duffy, M. B. Hunter, J. M. Byrne, P. Kelehan, H. J. Byrne, *Exp. Mol. Pathol.* **2007**, *82*, 121.
[37] Z. W. Huang, A. McWilliams, S. Lam, J. English, D. I. McLean, H. Lui, H. Zeng, *Int. J. Oncol.* **2003**, *23*, 649.
[38] T. J. Vickers, R. E. Wambles, C. K. Mann, *Appl. Spectrosc.* **2001**, *55*, 389.
[39] G. A. Wagnieres, W. M. Star, B. C. Wilson, *Photochem. Photobiol.* **1998**, *68*, 603.
[40] S. Svanberg, Atomic and Molecular Spectroscopy: Basic Aspects and Practical Applications, Springer Verlag, New York, **2004**.
[41] H. J. Rabal, R. A. Braga, Dynamic Laser Speckle and Applications, Taylor & Francis, New York, **2010**.
[42] R. L. McCreery, Raman Spectroscopy for Chemical Analysis, John Wiley & Sons, New York, **2005**.
[43] K. N. Liou, An Introduction to Atmospheric Radiation, Academic Press, New York, **2002**.
[44] T. Vo-Dinh, Biomedical Photonics Handbook, Taylor & Francis, New York, **2010**.
[45] L. V. Wang, H. Wu, Biomedical Optics: Principles and Imaging, John Wiley & Son, New York, **2012**.
[46] C. Nelson, J. Crist, *Laser Tech. J.* **2012**, *9*, 36.
[47] O. Svelto, D. D. C. Hanna, Principles of Lasers, Springer Verlag, New York, **2010**.
[48] W. T. Silfvast, Laser Fundamentals, Cambridge University Press, New York, **2004**.
[49] Z. M. Chen, R. Butke, B. Miller, C. L. Hitchcock, H. C. Allen, S. P. Povoski, E. W. Martin, J. V. Coe, *J. Phys. Chem. B* **2013**, *117*, 12442.

Supporting information

Additional supporting information may be found in the online version of this article at the publisher's web site.